DFT Analysis of Ca-doped $LiFePO_4$ Cathode Material for High-Performance Li-ion Batteries

Shahrul Izwan Ahmad[1], Ahmad Fairoz Aziz[2], Fadhlul Wafi Badrudin[1]*, Mohd Junaedy Osman[1], Mohd Syazwan Mohamad Anuar[1], Mohamad Fariz Mohamad Taib[3] and Muhd Zu Azhan Yahya[4]

[1]Centre for Defence Foundation Studies, Universiti Pertahanan Nasional Malaysia, 57100 Kuala Lumpur, Malaysia

[2]Department of Physics, Faculty of Applied Sciences, Universiti Teknologi MARA (UiTM), 26400 Jengka, Pahang, Malaysia

[3]Faculty of Applied Sciences, Universiti Teknologi MARA (UiTM), 40450, Shah Alam, Malaysia

[4]Faculty of Defence Science and Technology, Universiti Pertahanan Nasional Malaysia, 57000 Kuala Lumpur, Malaysia

*Corresponding author (e-mail: fadhlul@upnm.edu.my)

This study investigates the effects of calcium (Ca) doping on lithium iron phosphate ($LiFePO_4$) using the first principles method. Despite its stability and safety, its practical use is limited by low electronic conductivity and sluggish lithium ion diffusion. To address this issue, density functional theory (DFT) simulations were used to investigate how Ca doping influences the mechanical, electrical, and electrochemical properties of $LiFePO_4$. The results demonstrated that Ca doping reduced the energy gap of $LiFePO_4$ and $FePO_4$ to 2.164 eV and 1.110 eV, which led to better electron transport and improved electronic conductivity in the cathode material. Additionally, it increased the lithium diffusion coefficient from 1.04×10^{-11} $cm^2\ s^{-1}$ to 1.75×10^{-10} $cm^2\ s^{-1}$, which improved lithium ion mobility and rate capability. There was a slight expansion in lattice parameters which may facilitate better lithium diffusion pathways. Based on its mechanical properties, Ca-doped $LiFePO_4$ remained stable and there was increased ductility and isotropy which may help prevent microcrack formation during prolonged electrochemical cycling. Overall, the modification enhanced the performance of the $LiFePO_4$ cathode material, paving the way for advancements in battery technology.

Keywords: Cathode material; lithium-ion battery; calcium; doping; $LiFePO_4$

Received: July 2025; Accepted: August 2025

Since its discovery by Padhi and coworkers of John B. Goodenough in 1996, lithium iron phosphate ($LiFePO_4$) has emerged as a promising cathode material for rechargeable lithium-ion batteries due to its inherent safety, stability, and environmental friendliness [1]. This olivine LFP ($LiFePO_4$) has a lithium intercalation potential of 3.5 V with a theoretical capacity of 170 $mAhg^{-1}$ [2]. Despite these advantages, LFP suffers from low electronic conductivity (~10^{-9}–10^{-10} S cm^{-1}) and sluggish lithium ion diffusion rates (~10^{-14} $cm^2\ s^{-1}$, which limits its use in high-power applications [3–5]. To improve these properties, various strategies have been explored, including surface carbon coating, nanosizing, and doping with various elements [6–9].

Among these, carbon coating is the most widely used due to its cost-effectiveness and ease of large-scale production. This approach enhances conductivity by encapsulating the LFP surface and forming an electronic conductive network. Generally, the surface modification approach does not interfere with the internal material and has no significant impact on the material's intrinsic problems. LFP's poor conductivity is mainly due to its structure which only allows one dimensional lithium diffusion, leading to sluggish ion diffusion [10–12]. Despite the strong covalent P–O bond which stabilizes the structure, this characteristic hinders Li^+ transport into the PO_4^{3-} polyanion, thereby restricting the pathway to a single dimension. Moreover, the absence of a continuous network of Fe–O inside the crystal structure contributes to low electron conductivity [13].

Doping has been explored as an alternative strategy to modify the electronic structure of LFP and enhance its electrochemical performance. Various dopants, including transition metals (Mn, Co, V, Nb, Cr), heteroatoms (F, Cl, S), and alkali/alkaline earth metals (Na, K, Ca), have been investigated to understand the effects of doping on the properties of $LiFePO_4$ [14–20].

Among the potential dopants, calcium (Ca) has gained attention due to its favourable impact on the structural and electronic properties of the cathode material. Qu and coworkers [21] investigated the effect of Ca doping on the performance of Li_2FeSiO_4/C. They found that Ca doping significantly improved

the electrochemical properties of the Li_2FeSiO_4/C material. With the introduction of Ca atoms, there was a noticeable enhancement in structural stability, which in turn improved the material's electronic conductivity, effectively reduced the charge-transfer resistance, and increased the diffusion coefficient of lithium ions, which may lead to better capacity retention and rate capability. Previous work on Ca doping in $LiMnFePO_4$ showed that it significantly enhanced battery performance [22]. Ca doping increases electronic conductivity and the lithium ion diffusion coefficient, resulting in improved overall conductivity and faster transport within the material. Moreover, Ca-doped $LiMnFePO_4$ exhibits superior cycling stability, maintaining higher capacities over more charge-discharge cycles compared to its undoped counterpart. Kugnatahan et. al [23] studied the effects of various doping elements. They found that Ca doped at the Fe site of LFP was thermodynamically stable with a solution energy of -0.42 eV, making Ca the most favourable dopant among alkali-earth metals like Mg, Sr, and B, partly due to the ionic radius (1.00 Å) of Ca^{2+} which is close to that of Fe^{2+} (0.78 Å), while its Bader charge (+1.60) is almost equal to that of Fe (+1.55). This suggests that synthesizing $Li(Fe,Ca)PO_4$ is feasible and could enhance the electrochemical properties of the LFP cathode material.

Despite promising results, systematic computational studies on Ca-doped $LiFePO_4$ remain limited. This study aims to bridge that gap by using density functional theory (DFT) simulations to analyse how Ca doping affects the structural, electronic, and electrochemical properties of $LiFePO_4$. This study investigates how Ca incorporation alters the lattice structure, electronic properties, and lithium-ion migration energy of LFP, which can provide new insights into the potential of Ca-doped LFP for high-performance lithium-ion batteries.

METHODOLOGY

In this work, computational studies were carried out based on density functional theory (DFT) implemented in the Cambridge Serial Total Energy Package (CASTEP) [24] computer code available in Material Studio software. The spin-polarized general gradient approximation (GGA) with Perdew-Burke-Ernzerhof (PBE) [25] was used for the exchange-correlation function. The ultrasoft pseudopotential was used to model valence-electron interactions with Li $1s^1 2s^2$, O $2s^2 2p^4$, P $3s^2 3p^3$, Fe $3d^6 4s^2$, and Ca $3s^2 3p^6 4s^2$ considered as valence electron configurations. The effective Hubbard U parameter of U = 4.3 eV was set to the Fe 3d electronic state to correct the famous underestimation of the electronic band gap by conventional DFT, known as the GGA + U method. The plane wave cut-off energy was set to 650 eV and the Monkhorost-Pack scheme k-point of 1×1×1 was employed for the integration of the Brillouin zone. A supercell of 1×2×2 was used, which comprised of four units of LFP cells ($Li_{16}Fe_{16}P_{16}O_{64}$) with 112 atoms. One of the Fe atoms was replaced by a Ca atom representing 6.25 % impurities, which was the lowest Ca concentration at the Fe site that could be obtained in this system. The chosen cell size provided a practical balance between representing the doped system accurately and maintaining computational efficiency. While experimental studies typically investigate Ca doping levels in the range of 1–5 % [21, 22, 26], slightly higher concentrations are often employed in theoretical studies due to the computational costs associated with larger supercells required for lower dopant levels. The $FePO_4$ (FP) structure was constructed by removing all the lithium ions from the cell. The Broyden–Fletcher–Goldfarb–Shanno (BFGS) algorithm was used in the geometry optimization process until the self-consistent-field (SCF) convergence condition was reached. The energy change per atom was set to 2×10^{-5} eV, the maximum force to 0.05 eV/A, the maximum stress to 0.1 GPa, and the maximum displacement of atoms to 0.002 A. To calculate the migration energy of the lithium ion, the nudge elastic band (NEB) [27] calculation was carried out using Transition State Theory, which is available in CASTEP.

RESULTS AND DISCUSSION

Structural and Mechanical Properties

LFP formed crystals with an orthorhombic structure and *Pnma* space groups (no. 62). In its primitive cell, it contained four formula units ($Li_4Fe_4P_4O_{16}$). The cell was formed by FeO_6 octahedra which were connected to PO_4 tetrahedra by edge-sharing. This created a one-dimensional lithium-ion channel in the (010) plane along the *y*-axis for it to intercalate and deintercalate throughout the cathode material. Figure 1 shows the crystal structure of LFP and Ca-LFP. The structure was constructed based on experimental data obtained from XRD refinement analysis with lattice parameters a = 10.349 Å, b = 6.031 Å, c = 4.722 Å, and volume, V = 294.718 $Å^3$ [28]. The FP structure was created simply by removing the lithium ions in the cathode material.

To understand the effects of Ca substitution on structural properties, the lattice parameters of LFP before and after substitution were calculated. Table 1 shows the calculated lattice parameters of LFP and Ca-LFP in comparison with other theoretical and experimental data. For LFP and FP, the current work slightly overestimates the experimental lattice parameters. This is due to the effect of the Hubbard U parameter that tends to slightly overestimate lattice parameters and volume. The results are still acceptable and in agreement with previous theoretical studies [29]. Upon substituting the Fe atom with a Ca atom, the lattice parameters of LFP increased slightly. This is expected as the ionic radius of Ca^{2+} (1.00 Å) is bigger than that of Fe^{2+} (0.78 Å) [30]. Structural expansion provides a wider pathway for lithium diffusion, which should improve the charge/discharge rate.

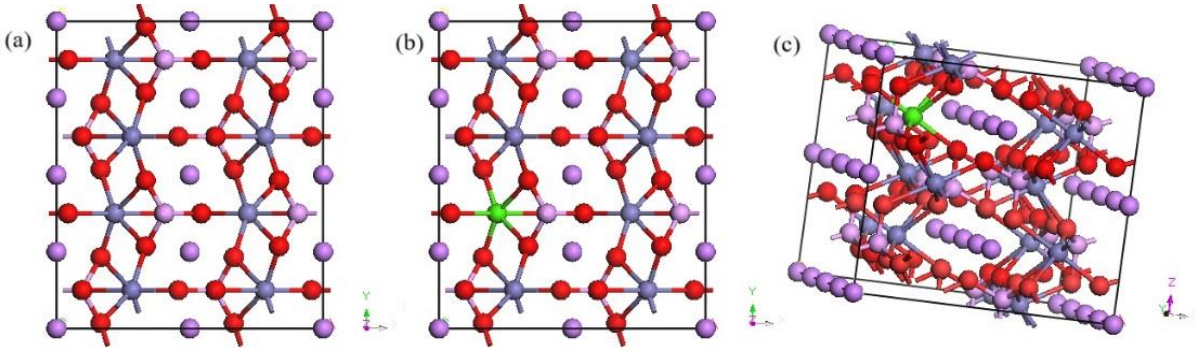

Figure 1. Crystal structures of (a) LFP, (b) Ca-LFP and (c) perspective view of Ca-LFP. The lithium ions, oxygen atoms, iron atoms, phosphorus atoms and calcium atoms are in purple, red, grey, pink and green, respectively.

Charging and discharging involves the extraction and insertion of lithium ions into the cathode material. During this process, the cathode undergoes contraction and expansion. This recurring process can degrade the battery and reduce its life cycle. Too much expansion can lead to instability and structural collapse. As lithium is extracted from the cathode material, the Fe^{2+} (0.78 Å ionic radius) is oxidized to Fe^{3+} (0.65 Å) causing shrinkage of the cathode material. This is one of the reasons why FP has a smaller volume compared to LFP.

The delithiation process reduced the calculated volume of Ca-LFP by 2.56 %. This is because the Ca^{2+} ion which replaced the Fe^{2+} does not oxidize during delithiation. As the amount of Fe^{3+} was reduced, the volume change was limited. With this behaviour, the life cycle of LFP should improve with Ca doping. However, there may be small reductions in theoretical capacity (160 $mAhg^{-1}$) as Ca^{2+} does not contribute to the redox reaction of Fe^{2+}/Fe^{3+} which the battery depends on. Nonetheless, this reduction will be compensated by the increase in electronic and ionic conductivity, which will be discussed later.

Formation energy, E_f, represents the energy change when a compound is formed from its basic elements in their standard state. Evaluating the formation energy is important to determine the thermodynamic stability of the doping system. The lower the formation energy, the more stable the system [32]. Formation energy is calculated based on Eq. (1), where E_{total} is the total energy of the doped system, E_{LFP} is the total energy of pristine LFP, and E_{Fe} and $E_{Ca}$are the chemical potentials of iron and calcium, respectively.

$$E_f = E_{total} - E_{LFP} + E_{Fe} - E_{Ca} \quad (1)$$

The formation energy for this doped system was -4.07 eV. Compared to previous studies which substituted different elements, this calculated value is acceptable [16,33,34]. Thus, this doped system is feasible and a thermodynamically stable system.

Table 1. Comparison of the lattice parameters of LFP and Ca-LFP with other theoretical and experimental data.

	a (Å)	2*b* (Å)	2*c* (Å)	V (Å)	ΔV (Å)	Ref
[a] $LiFePO_4$	10.33	12.02	9.39	1166.48	6.60 %	[31]
[a] $FePO_4$	9.82	11.58	9.58	1089.44		[31]
[b] $LiFePO_4$	10.44	12.14	9.49	1204.24	3.42 %	[29]
[b] $FePO_4$	9.986	11.82	9.762	1152.84		[29]
[b] $LiFePO_4$	10.44	12.15	9.48	1202.70	4.61 %	current work
[b] $FePO_4$	9.93	11.85	9.75	1147.28		current work
[b] Ca-$LiFePO_4$	10.45	12.16	9.48	1205.01	2.56 %	current work
[b] Ca-$FePO_4$	9.97	11.96	9.84	1174.12		current work

[a] experimental, [b] theoretical

Table 2. Calculated elastic constants of LFP and Ca-LFP (in GPa).

	C_{11}	C_{22}	C_{33}	C_{44}	C_{55}	C_{66}	C_{12}	C_{13}	C_{23}	Ref
LFP-cal.	138.9	198.0	173.0	36.8	50.6	47.6	72.8	52.5	45.8	[37]
LFP-cal.	149.1	187.0	178.2	39.1	50.2	46.7	71.4	58.9	48.0	[16]
LFP	140.0	182.4	169.5	37.8	47.2	48.8	67.3	53.4	44.2	current work
Ca-LFP	134.0	179.2	163.4	39.0	44.6	46.7	66.6	55.4	45.1	current work

The electrochemical performance of a cathode material relies on the stability of its material. Instability can lead to phase transformation and degradation. These can reduce the charge and discharge efficiency of the battery. To ddetermine material stability, the elastic constant, C_{ij} is calculated. The elastic constant is commonly used to state the relationship between stress and strain in a material. Under the conditions of the elastic limit and small strains, C_{ij} serves as an indicator of the material's mechanical stability. In an orthotropic system, the elastic constants C_{11}, C_{22}, and C_{33} represent the linear compressive moduli along the X, Y, and Z direction respectively. C_{44}, C_{55}, and C_{66} correspond to the shear moduli in the (100), (010), and (001) planes, while C_{12}, C_{13}, and C_{23} are related to longitudinal and transverse contractions.

The calculated elastic constants C_{ij} for LFP and Ca-LFP are presented in Table 2. According to the Born criterion, an orthotropic crystalline system is mechanically stable if it satisfies the following conditions, [35, 36]:

$$C_{11} > 0,\ C_{22} > 0,\ C_{33} > 0,\ C_{44} > 0,\ C_{55} > 0,\ C_{66} > 0,\ C_{11} + C_{22} + C_{33} + 2(C_{12} + C_{13} + C_{23}) > 0,\ (C_{11} + C_{22} - 2C_{12}) > 0,\ (C_{11} + C_{33} - 2C_{13}) > 0,\ (C_{22} + C_{33} - C_{23}) > 0 \quad (2)$$

Based on the calculated lattice constants in Table 2, both LFP and Ca-LFP meet the stability conditions. This suggests that Ca doping is practical and does not reduce mechanical stability. To further evaluate the mechanical properties, two standard methods, the Voigt and Reuss methods, were employed to determine the bulk and shear moduli of LFP and Ca-LFP. The Voigt method assumes uniform strain, while the Reuss method assumes uniform stress. These two methods determine the upper and lower limits of the elastic modulus of the polycrystalline material. By averaging both values, the more accurate expression of bulk modulus, B and shear modulus, G can be obtained.

$$B = \frac{B_V + B_R}{2} \quad (3)$$

$$G = \frac{G_V + G_R}{2} \quad (4)$$

The bulk modulus and shear modulus are then used to compute the Young's modulus, E, and Poisson's ratio, v, using the following equations [35]:

$$E = \frac{9BG}{3B + G} \quad (5)$$

$$v = \frac{3B - 2G}{6B + 2G} \quad (6)$$

Table 3 provides a comparison of the mechanical properties of LFP and Ca-LFP. The bulk modulus reflects resistance to uniform compression, while the shear modulus indicates resistance to shear deformation, with higher values indicating greater material stiffness. Young's modulus highlights the material's resistance to deformation under stress. Prior to doping, there was a slight decrease in the mechanical properties (B, G, E) of LFP, signifying a small reduction in strength, stiffness, and ductility. In terms of Poisson's ratio, the Ca-LFP showed shear-induced deformation properties similar to LFP. The Pugh criterion, which is the ratio of B/G, was also used to assess material ductility and brittleness. A value above 1.75 indicates ductile behaviour, while a lower value indicates brittleness. For LFP and Ca-LFP, the B/G ratios were 1.91 and 1.95 respectively. This shows that Ca doping improved the ductility of the cathode material. Higher ductility indicates that the cathode material is less prone to cracking during prolonged cycling, which is important for its stability and efficiency.

Table 3. Shear Modulus (G), Bulk Modulus (B), Young Modulus (E), Poisson Ratio (v) and Pugh Criterion, B/G values. G, B and E are in GPa.

	G_R	G_V	G	B_R	B_V	B	E	v	B/G	Ref.
LFP	48.6	46.9	47.7	91.3	90.6	91.0	121.9	0.30	1.91	Present work
Ca-LFP	46.7	45.2	46.0	90.1	89.3	89.7	117.8	0.30	1.95	Present work
LFP-cal.	47.2	49.6	48.4	93	94.7	93.9	123.9	0.28	1.94	[37]
LFP-cal.	49.2	51.1	50.2	96.5	97.1	96.8	128.9	0.28	1.93	[32]

Microcracks or deformations may develop in materials due to crystal anisotropy. This behaviour has previously been discovered in LFP particles, and becomes more frequent with prolonged cycling [38]. One of the factors that might contribute to these defects is elastic anisotropy. To calculate this effect, Ranganathan et al. [39] introduced a universal elastic anisotropy index (A^U):

$$A^U = 5\frac{G_V}{G_R} + \frac{B_V}{B_R} - 6 \quad (5)$$

where G_V, G_R, B_V and B_R represent the calculated values from the Voigt and Reuss methods. Isotropy is present in a crystal if $A^U = 0$. If the value is greater than 0, the degree of anisotropy will increase in the crystal structure. In the present study (Table 4), the anisotropy index of LFP was 0.19, in agreement with previous work [32]. After Ca substitution, the index reduced to 0.17, indicating an increase in the degree of isotropy. Another anisotropy factor which has been defined by Chung and Buessem [40] is as follows:

$$A_B = \frac{B_V - B_R}{B_V + B_R} \quad (6)$$

$$A_G = \frac{G_V - G_R}{G_V + G_R} \quad (7)$$

The more the value approaches zero, the more isotropic the material. The values obtained after doping suggest that the material's isotropy remained Unchanged (Table 4). The following are shear anisotropy factors by Ravindran.

$$A_1 = 4C_{44}/(C_{11} + C_{33} - 2C_{13}) \quad (8)$$

$$A_2 = 4C_{55}/(C_{22} + C_{33} - 2C_{23}) \quad (9)$$

$$A_3 = 4C_{66}/(C_{11} + C_{22} - 2C_{12}) \quad (10)$$

These provide a measure of the degree of anisotropy in the bonding between atoms in different planes [41]. A_1 is for the (100) shear plane in the ⟨010⟩ and ⟨011⟩ directions, A_2 for the (010) shear plane in the ⟨001⟩ and ⟨101⟩ directions, and A_3 for the (001) shear plane in the ⟨010⟩ and ⟨110⟩ directions. If the values of A_1, A_2, and A_3 are equal to 1, the material will exhibit isotropy, and the more the value deviates from 1, the higher the degree of anisotropy. As can be seen in Table 4, prior to doping with Ca, LFP exhibited some degree of anisotropy in the (100) and (010) planes and tended to be isotropic in the (001) plane. After Ca doping, there was an improvement in the degree of isotropy in the (100) plane. In the (010) and (001) planes, no significant change was observed. Overall, Ca doping positively improved the degree of isotropy in LFP which lowers the likelihood of microcrack formation. It must be noted that a tiny crack can negatively degrade the electrochemical performance of the cathode material. Previous work has shown that microcracks caused some LFP particles to be electronically disconnected and suffer a loss in capacity [42]. Thus, improving the degree of isotropy should help to improve the life cycle of the cathode material.

Table 4. Shear Anisotropy Factors (A_1, A_2 and A_3), Elastic Anisotropy (A_B and A_G) and Universal Elastic Anisotropy index (A_U).

	LFP	**Ca-doped**	**LFP** [16]	**LFP** [32]	**LFP** [37]
A_1	0.75	0.84	0.74	0.73	0.712
A_2	0.61	0.60	0.74	0.77	0.724
A_3	1.04	1.04	0.96	1.06	0.995
A_B	0.00	0.00	-	0.003	-
A_G	0.02	0.02	-	0.0019	-
A_U	0.19	0.17	-	0.20	-

Electronic Properties

As mentioned in a previous work by Zhang et al., the major factor for determining the electronic conductivity of a solid is the band gap [43]**.** This energy gap can be obtained from the density of state calculation. Figure 2 displays the density of state of LFP and FP. In between the conduction bands and valence bands of LFP and FP, there is an energy gap of 3.696 eV and 1.447 eV, respectively. These values are in agreement with previous theoretical and UV-Vis experimental data [34, 44, 45]. The calculated results were generated using a Hubbard U parameter with a value of 4.3 eV. Without it, the calculated energy gap would be underestimated by about 0.5 eV for LFP, which would incorrectly indicate this cathode material as metallic. Incorporation of Hubbard U overcomes the incomplete cancellation of the electronic self-interaction error of the delocalized 3*d* state. The energy gap of 3.696 eV can be considered as a wide band gap, impeding the self-generation of electrons or holes. This drawback gives LFP insulating behaviour leading to poor electronic conductivity, which is the main problem with LFP cathode materials. To solve this issue, foreign impurities may be introduced into the cathode material to tune its conductivity.

Figure 3 displays the calculated density of state of Ca-LFP and Ca-FP. The presence of Ca as a dopant altered the electronic structure of LFP. There was a small contribution from Ca state to the density of state, particularly at the conduction band. The Ca state weakly overlapped with the Fe state and seemed to play a role in reducing the energy gap of LFP and FP to 2.164 eV and 1.110 eV, respectively. As can be seen in the Figure 2 (a), with the involvement of the Ca state, the Fe state in LFP, a prominent peak at ~5 eV shifted to ~2.5 eV (Figure 3 (a)). This reduced gap allows electrons to easily transition from the valence band to the conduction band, as less energy is required [9, 16, 19].

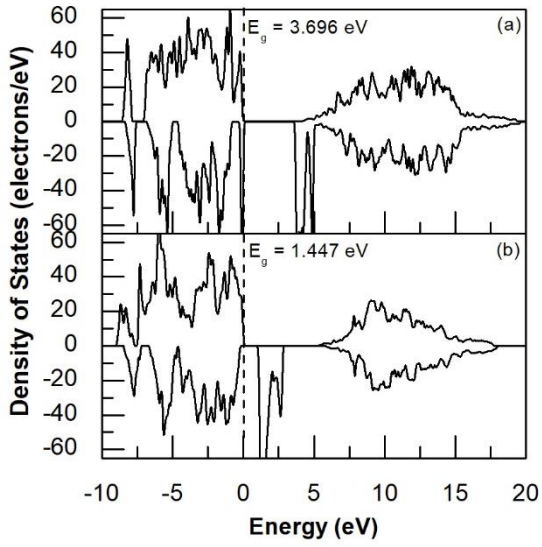

Figure 2. The density of state (DOS) of (a) LFP and (b) FP.

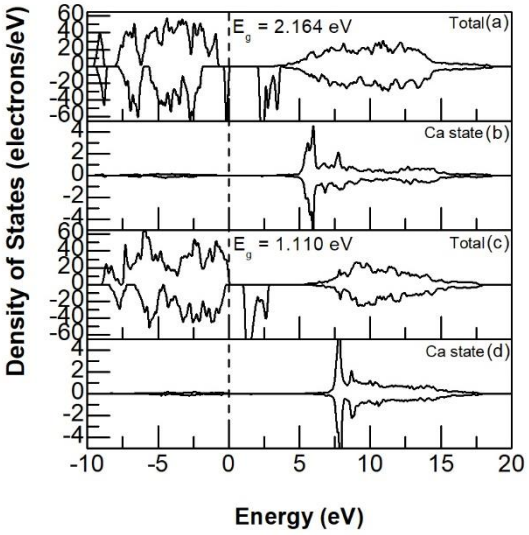

Figure 3. The calculated DOS of Ca-LFP and Ca-FP: (a)The DOS of Ca-LFP, (b) the Ca atom state in the LFP DOS, (c) the DOS of Ca-FP and (b) Ca atom state in the FP DOS.

The reduction in the energy gap implies higher electrical conductivity. This is in agreement with previous work. Liu et al. [22] performed Ca doping on $LiFe_{0.5}Mn_{0.5}PO_4$ and found that it greatly increased electronic conductivity by reducing charge transfer resistance, and increased lithium-ion diffusion. Similar trends were also found by Fey et al. [26] in their work on a Ca doped LFP which showed an increase in electronic conductivity and lithium-ion diffusion. This confirms that Ca doping effectively improved the electrochemical performance of LFP.

It is worth noting that although the electronic conduction in $LiFePO_4$ is dominated by thermally activated polaron hopping rather than intrinsic band conduction [46], the calculated energy gap, E_g is often used as a qualitative descriptor of electronic conductivity. In intrinsic semiconductors, the carrier concentration, and thus the conductivity, σ follow an Arrhenius-type dependence, $\sigma \propto \exp\left(-\frac{E_a}{kT}\right)$, where $E_a \approx E_g/2$. This means that a narrower band gap corresponds to higher conductivity. While this relationship does not strictly apply to polaronic materials, dopant-induced band gap narrowing in $LiFePO_4$, generally indicates the formation of intermediate states closer to Fermi level, which reduces the energy gap, E_g and effective activation energy, E_a for polaron hopping and thereby enhances electronic conductivity. This has been demonstrated in previous work by Chung at al. [47] on Mg, Zr and Nb doping, which showed that the activation energy was reduced to ~60-80 meV compared to undoped $LiFePO_4$ (500 meV), and this was accompanied by an improvement in conductivity.

Lithium Migration

In addition to electronic conductivity, ionic conductivity also plays an important role in the electrochemical performance of the cathode material, especially in terms of rate capability. This is related to Li ion mobility inside the cathode material which can be probed via the migration energy, E_m calculated based on transition state. Figure 4 shows the comparison of the migration energy of LFP and Ca-LFP along the [010] direction. This direction is the most stable pathway and is responsible for lithium ion diffusion in the LFP cathode material [48]. The migration energy path looks arch-like due to electrostatic interactions between Li and its neighbouring Fe or Ca ion. Prior to doping the migration energy of the lithium ion was 0.532 eV. After Ca doping, the migration energy reduced to 0.459 eV. This value can be used to calculate the diffusion coefficient, D using the Arrhenius equation below:

$$D = a^2 v \exp\left(-\frac{E_m}{k_B T}\right) \quad (11)$$

where a is the jump distance along the b-axis (3.0 Å), v is attempt frequency (10^{13} Hz), k_B is the Boltzmann constant, T is the temperature of the system (300 K), and E_m is the migration energy.

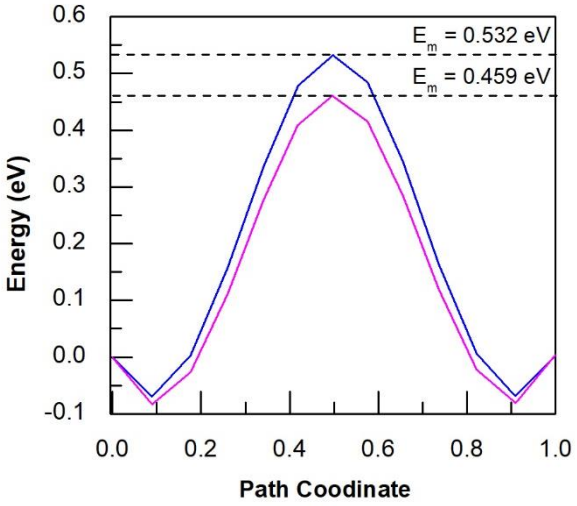

Figure 4. The migration energy of the Li ions in LFP (blue line) and Ca-LFP (pink line).

Table 5. Calculated Diffusion Coefficients for LFP and Ca-LFP using the Arrhenius Equation.

	Migration Energy, E_m (eV)	**Diffusion Coefficient, D (cm^2s^{-1})**
LFP	0.532	1.04×10^{-11}
Ca-LFP	0.459	1.75×10^{-10}

*Parameters use: a = 3.0 Å, $v = 10^{13}$ Hz and T = 300 K

For LFP and Ca-LFP the calculated diffusion coefficients (Table 5) were 1.04×10^{-11} cm^2 s^{-1} and 1.75×10^{-10} cm^2 s^{-1}, respectively. This indicates that Ca doping improved the ionic conductivity of the lithium ion. This has been shown in a previous study where $LiFeMnPO_4$ demonstrated higher diffusion coefficients compared to $LiFePO_4$ during the discharge process [22]. Zhang et al. also demonstrated that Ca doping in $LiFePO_4$ significantly accelerated lithium migration due to broadening of the lithium-ion migration pathway [49]. Ca doping increased the lattice parameters and volume of LFP and provided an easy pathway for lithium migration. This is known as the "pillar effect" which reduces energy barriers for lithium ion diffusion, making it easier for them to move within the material [50], thus increasing the diffusion rate and enhancing the rate performance of the cathode.

CONCLUSION

The effects of Ca doping on the LFP cathode material were investigated. It was found that Ca doping improved mechanical and electrochemical performance. Ca-LFP satisfied the thermodynamic stability requirements, which indicated that this doping system was feasible. Based on the stability conditions, Ca doping did not compromise mechanical stability. Even with a slight decrease in mechanical properties (B, G, E), there was an improvement in ductility and the degree of isotropy, which should prevent microcrack formation after prolonged usage. In terms of electronic properties, the energy gap values for LFP and FP were reduced to 2.164 eV and 1.110 eV, indicating improved electronic conductivity. Moreover, based on transition state theory, the migration energy of Ca-doped LFP reduced from 0.532 eV to 0.459 eV. This contributed to an increase in the diffusion coefficient from 1.04×10^{-11} cm^2 s^{-1} to 1.75×10^{-10} cm^2 s^{-1}, indicating faster lithium ion diffusion, which should offer a higher rate capability. To further confirm these results, experimental synthesis and electrochemical testing should be performed in the future. Other explorations such as a defect study, and doping optimization should also be attempted to seek deeper insights into the practical implementation of a doping strategy for next generation energy storage devices.

ACKNOWLEDGEMENTS

This work was supported by an internal UPNM grant (Grant code: UPNM/2021/GPJP/STG/2). The authors would like to express their gratitude to the Core Group for Academic Development and Research Experts (CADRE), in the Centre for Defence Foundation Studies, Universiti Pertahanan Nasional Malaysia.

REFERENCES

1. Padhi, A. K., Nanjundaswamy, K. S. and Goodenough, J. B. (1997) Phospho-olivines as Positive-Electrode Materials for Rechargeable Lithium Batteries. *J. Electrochem Soc*., **144**, 1188–1194.

2. Wang, J. and Sun, X. (2015) Olivine $LiFePO_4$: the remaining challenges for future energy storage. *Energy Environ Sci*., **8**, 1110–1138.

3. Liu, Q., Wen, D., Yu, X. and Jiang, H. (2023) Effect of Na-Si co-doping on the performance of LiFePO4, *Journal of Electroanalytical Chemistry*, **950**.

4. Ahmad, S. I., Badrudin, F. W., Abdullah, A. L. A., Yahya, M. Z. A., Taib, M. F. M. and Hassan, O. H. (2022) Evaluation of Olivine LiFePO4 Polyanionic Cathode Material Using Density Functional Theory. *Key Eng. Mater*., **908**, 293–298.

5. Yao, C., Wang, F., Chen, J. and Yin, M. (2022) First-principles study of the structural and electronic properties of LiFePO4 by graphene and N-doped graphene modification. *Comput. Theor. Chem*., **1217**, 113897.

6. Lee, J., Oh, J., Jeon, Y. and Piao, Y. (2018) Multi-Heteroatom-Doped Hollow Carbon Attached on Graphene Using LiFePO 4 Nanoparticles as Hard Templates for High-Performance Lithium–Sulfur Batteries. *ACS Appl. Mater. Interfaces*., **10**, 26485–26493.

7. Li, Y., Wang, L., Zhang, K., Liang, F., Yuan, M., Zhang, H. and Yao, Y. (2021) An encapsulation of phosphorus doped carbon over LiFePO4 prepared under vacuum condition for lithium-ion batteries. *Vacuum*., **184**, 109935.

8. Zhang, Y., Alarco, J. A., Nerkar, J. Y., Best, A. S., Snook, G. A., Talbot, P. C. and Cowie, B. C. C. (2020) Observation of Preferential Cation Doping on the Surface of LiFePO4Particles and Its Effect on Properties. *ACS Appl. Energy Mater*., **3**, 9158–9167.

9. Chen, Z., Wang, F., Li, T., Wang, S., Yao, C. and Wu, H. (2024) First-principles study of LiFePO4 modified by graphene and defective graphene oxide. *J. Mol. Graph Model*, **129**.

10. Luo, G. Y., Gu, Y. J., Liu, Y., Chen, Z. L., Lin Huo, Y., Wu, F. Z., Mai, Y., Dai, X. Y. and Deng, Y. (2021) Electrochemical performance of in situ LiFePO4 modified by N-doped graphene for Li-ion batteries. *Ceram Int*., **47**, 11332–11339.

11. Chou, S. K., Birgersson, K. E., Balaya, P., Yan, J. and Adams, S. (2012) Ultrafast lithium migration in surface modified LiFePO4 by heterogeneous doping. *Appl. Energy*., **90**, 323–328.

12. Xu, G., Zhong, K., Zhang, J. and Huang, Z. (2014) First-principles investigation of the electronic and Li-ion diffusion properties of LiFePO 4 by sulfur surface modification. *J. Appl. Phys*., **116**, 063703.

13. Yang, L., Deng, W., Xu, W., Tian, Y., Wang, A., Wang, B., Zou, G., Hou, H., Deng, W. and Ji, X. (2021) Olivine LiMnxFe1−xPO4 cathode materials for lithium ion batteries: restricted factors of rate performances. *J. Mater. Chem. A. Mater*., **9**, 14214–14232.

14. Zaki, N. H. M., Ahmad, S. I., Sazman, F. N., Badrudin, F. W., Abdullah, A. L. A., Taib, M. F. M., Hassan, O. H. and Yahya, M. Z. A. (2023) The influence of Cl doping on the structural, electronic properties and Li-ion migration of LiFePO4: A DFT study. *Comput. Theor. Chem*., **1221**, 114029.

15. Kanungo, S., Bhattacharjee, A., Bahadursha, N. and Ghosh, A. (2022) Comparative Analysis of LiMPO4 (M = Fe, Co, Cr, Mn, V) as Cathode Materials for Lithium-Ion Battery Applications—A First-Principle-Based Theoretical Approach. *Nanomaterials*, **12**.

16. Wang, S. and Wang, F. (2023) Effect of Mn, N co-doped LiFePO4 on electrochemical and mechanical properties: A DFT study. *J. Mol. Graph Model*, **125**, 108604.

17. Xiao-Fang, O., Si-Qi, S., Chu-Ying, O., Di-You, J., De-Sheng, L., Zhi-Qing, Y. and Min-Sheng, L. (2007) First principles studies on the electronic structures of Li M_x Fe $_{1-x}$ PO $_4$ (M = Co, Ni and Rh). *Chinese Physics*, **16**, 3042–3045.

18. Omenya, F., Chernova, N. A., Upreti, S., Zavalij, P. Y., Nam, K. -W., Yang, X. -Q. and Whittingham, M. S. (2011) Can Vanadium Be Substituted into LiFePO4? *Chemistry of Materials*, **23**, 4733–4740.

19. Lv, Z., Li, M., Yang, H., Lin, J., Luo, J., Hong, R., Wu, B. and Cao, S. C. (2024) The first-principles study on electrochemical performance, mechanical properties, and lithium-ion migration of LiFePO4 modified by doping with Co and Nb. *Journal of Solid State Electrochemistry*, **28**, 2873–2883.

20. Zhao, X., Wang, S., Wang, F. and Liu. S. (2024) Study on the Influence of Mn and Cl Co-Doping on the Electrochemical and Mechanical Properties of LiFePO4: A First-Principles Investigation. *High Energy Chemistry*, **58**, 469–479.

21. Qu, L., Li, M., Tian, X, Liu, P., Yi, Y. and Yang, B. (2018) Calcium cation enhanced cathode/electrolyte interface property of Li2FeSiO4/C cathode for lithium-ion batteries with long-cycling life. *Chem. Phys*., **503**, 1–13.

22. Liu, W., Liu, X., Hao, R., Yang, Z., Ouyε 10 B., Zhang, M., Pan, M. and Liu, K. (2023) Contribution of calcium ion doping to the rate property for LiFe0.5Mn0.5PO4/C. *Journal of Electroanalytical Chemistry*, **929**.

23. Kuganathan, N. and Chroneos, A. (2022) Formation, doping, and lithium incorporation in LiFePO4. *AIP Adv*., **12**.

24. Stewart J. Clark, Segall, M. D., Pickard, C. J., Hasnip, P. J., Probert, M. I. J., Refson, K. and Payne, M. C. (2005) First principles methods using CASTEP. *Zeitschrift Für Kristallographie*, **220**, 567.

25. Perdew, J. P., Burke, K. and Ernzerhof, M. (1997) Generalized Gradient Approximation Made Simple. *Phys. Rev. Lett*., **78**, 1396.

26. Fey, G. T. K., Yan, C. J., Lin, Y. C., Huang, K. P., Da Cho, Y., Wu, P. J., Sen Sun, Y. and Kao, H. M. (2012) Calcium Doping Effects on the Electrochemical Properties of LiFePO4/C Cathode Materials for Lithium-Ion Batteries. *Adv. Mat. Res*., **560–561**, 499–505.

27. Henkelman, G., Uberuaga, B. P. and Jónsson, H. (2000) A climbing image nudged elastic band method for finding saddle points and minimum energy paths. *J. Chem. Phys*., **113**, 9901–9904.

28. Streltsov, V. A., Belokoneva, E. L., Tsirelson, V. G. and Hansen, N. K. (1993) Multipole analysis of the electron density in triphylite, LiFePO 4, using X-ray diffraction data. *Acta Crystallogr B*., **49**, 147–153.

29. Laref, S. and Laref, A. (2015) Theoretical insight into the strain effect on the intercalation potential of Li-FePO4 materials. *RSC Adv.*, **5**, 35667–35674.

30. Shannon, R. D. (1976) Revised effective ionic radii in halides and chalcogenides. *Acta Crystallogr.*, **A32**, 751–767.

31. Lin, H., Wen, Y., Zhang, C., Zhang, L., Huang, Y., Shan, B. and Chen, R. (2012) A GGA+U study of lithium diffusion in vanadium doped LiFePO4. *Solid State Commun*., **152**, 999–1003.

32. Chen, J., Wang, F., Yin, M. and Yao, C. (2022) First-Principles Study on the Electronic Properties and Mechanical Stabilities of Anion-Cation Multiple-Doped LiFePO 4. *Chemistry Select*., **7**.

33. Jiao, L. X., Li, Z. Q., Zhu, Y. Z., Wei, Z., Liang, Y., Wang, X. L., Cui, Y., Zhang, Z. H., He, M. and Song, B. (2023) Enhanced electrical conductivity and lithium ion diffusion rate of LiFePO4 by Fe site and P site doping. *AIP Adv*., **13**.

34. Jiang, K., Wang, F., Liu, M., Fan, Y., Chen, Z., Li, G., Li, P., Shi, X. and Hong, W. (2024) First principles study of the electronic structure and Li-ion diffusion properties of co-doped LIFex-1MxPyNy-1O4 (M=Co/Mn, N=S/Si) Li-ion battery cathode materials. *Micro and Nanostructures*, **196**.

35. Wu, Z. J., Zhao, E. J., Xiang, H. P., Hao, X. F., Liu, X. J. and Meng, J. (2007) Crystal structures and elastic properties of superhard Ir N2 and Ir N3 from first principles. *Phys. Rev. B. Condens. Matter. Mater. Phys*., **76**.

36. Lethole, N. L., Chauke, H., Ngoepe, P. E., Lethole, N. L., Chauke, H. R. and Ngoepe, P. E. (2018) First-principles stability study of olivine NaMPO4 (M: Mn, Fe, Co). *In: Proceedings of SAIP2017, SA Institute of Physics*, 2018: 47–53.

37. Maxisch, T. and Ceder, G. (2006) Elastic properties of olivine Lix FePO4 from first principles. *Phys. Rev. B. Condens. Matter. Mater. Phys*., **73**, 1–4.

38. Wang, D., Wu, X., Wang, Z. and Chen, L. (2005) Cracking causing cyclic instability of LiFePO4 cathode material. *J. Power Sources*, **140**, 125–128.

39. Ranganathan, S. I. and Ostoja-Starzewski, M. (2008) Universal elastic anisotropy index. *Phys. Rev. Lett*., **101**.

40. Chung, D. H. and Buessem, W. R. (1967) The Voigt-Reuss-Hill Approximation and Elastic Moduli of Polycrystalline MgO, CaF2, β-ZnS, ZnSe, and CdTe. *J. Appl. Phys*., **38**, 2535–2540.

41. Ravindran, P., Fast, L., Korzhavyi, P. A., Johansson, B., Wills, J. and Eriksson, O. (1998) Density functional theory for calculation of elastic properties of orthorhombic crystals: Application to TiSi2. *J. Appl. Phys*., **84**, 4891–4904.

42. Scipioni, R., Jørgensen, P. S., Hjelm, J., Norby, P., Rasmussen, C. N. and Jensen, S. H. (2014) Degradation Studies on LiFePO 4 cathode. *ECS Meeting Abstracts*, **MA2014-02**, 382–382.

43. Zhang, Y., Alarco, J. A., Best, A. S., Snook, G. A., Talbot, P. C. and Nerkar, J. Y. (2019) Re-

evaluation of experimental measurements for the validation of electronic band structure calculations for LiFePO 4 and FePO 4, *RSC Adv*., **9**, 1134–1146.

44. Ahmad, S. I., Badrudin, F. W., Abdullah, A. L. A., Yahya, M. Z. A., Taib, M. F. M. and Hassan, O. H. (2022) Evaluation of Olivine LiFePO4 Polyanionic Cathode Material Using Density Functional Theory. *Key Eng. Mater*., **908**, 293–298.

45. Zaghib, K., Mauger, A., Goodenough, J. B., Gendron, F. and Julien, C. M. (2007) Electronic, Optical, and Magnetic Properties of LiFePO 4 : Small Magnetic Polaron Effects. *Chemistry of Materials*, **19**, 3740–3747.

46. Zhou, F., Kang, K., Maxisch, T., Ceder, G. and Morgan, D. (2004) The electronic structure and band gap of LiFePO4 and LiMnPO4. *Solid State Commun*., **132**, 181–186.

47. Chung, S. Y., Bloking, J. T. and Chiang, Y. M. (2002) Electronically conductive phospho-olivines as lithium storage electrodes. *Nat. Mater*., **1**, 123–128.

48. Bhandari, A., Gupta, P. K., Bhattacharya, J. and Pala, R. G. S. (2019) Higher Energy Barrier for Interfacial Li-Ion Transfer from EC/LiPF 6 Electrolyte into (010) LiFePO 4 Cathode Surface than Bulk Li-Ion Diffusion within Both Cathode and Electrolyte. *J. Electrochem. Soc*., **166**, A2966–A2972.

49. Zhang, Z., Ma, H. and Wan, B. (2025) Synthesis, Characterisation and Electrochemical Performance of Calcium Ion Doped LiFePO4 Cathodes in Phosphogypsum for Advanced Lithium Ion Batteries. *JOM*, **77**, 2943–2951.

50. Liu, L., Chen, G., Du, B, Cui, Y., Ke, X., Liu, J., Guo, Z., Shi, Z., Zhang, H. and Chou, S. (2017) Nano-sized cathode material LiMn0.5Fe0.5PO4/C synthesized via improved sol-gel routine and its magnetic and electrochemical properties. *Electrochim Acta*, **255**, 205–211.